Dental Materials 40 (2024) 593–607

Contents lists available at ScienceDirect

Dental Materials

journal homepage: www.elsevier.com/locate/dental

Natural, biphasic calcium phosphate from fish bones for enamel remineralization and dentin tubules occlusion

Lorenzo Degli Esposti [a], Andrei C. Ionescu [b,c], Sara Gandolfi [a,d], Nicoleta Ilie [e], Alessio Adamiano [a], Eugenio Brambilla [b], Michele Iafisco [a,*]

[a] Institute of Science, Technology and Sustainability for Ceramics (ISSMC), National Research Council (CNR), Via Granarolo 64, 48018 Faenza, Italy
[b] Oral Microbiology and Biomaterials Laboratory, Department of Biomedical, Surgical, and Dental Sciences, University of Milan, Via Pascal, 36, 20133 Milan, Italy
[c] Ospedale Maggiore Policlinico, Fondazione IRCCS Cà Granda, Milan 20100, Italy
[d] Dipartimento di Scienze Chimiche, della Vita e della Sostenibilità Ambientale, Parco Area delle Scienze 17/A, 43124 Parma, Italy
[e] Department of Conservative Dentistry and Periodontology, University Hospital, Ludwig-Maximilians-University, Goethestr. 70, 80336 Munich, Germany

ARTICLE INFO

Keywords:
Preventive dentistry
Natural calcium phosphates
Circular economy
Fish bones
Enamel remineralization
Dentin desensitization
Microindentation
Dynamic mechanical analysis

ABSTRACT

Objectives: A calcium phosphate extracted from fish bones (CaP-N) was evaluated for enamel remineralization and dentinal tubules occlusion.
Methods: CaP-N was characterized by assessing morphology by SEM, crystallinity by PXRD, and composition by ICP-OES. CaP-N morphology, crystallinity, ion release, and pH changes over time in neutral and acidic solutions were studied. CaP-N was then tested to assess remineralization and dentinal tubules occlusion on demineralized human enamel and dentin specimens (n = 6). Synthetic calcium phosphate in form of stoichiometric hydroxyapatite nanoparticles (CaP-S) and tap water were positive and negative controls, respectively. After treatment (brush every 12 h for 5d and storage in Dulbecco's modified PBS), specimens' morphology and surface composition were assessed (by SEM-EDS), while the viscoelastic behavior was evaluated with microindentation and DMA.
Results: CaP-N consisted of rounded microparticles (200 nm - 1 μm) composed of 33 wt% hydroxyapatite and 67 wt% β-tricalcium phosphate. In acidic solution, CaP-N released calcium and phosphate ions thanks to the preferential β-tricalcium phosphate phase dissolution. Enamel remineralization was induced by CaP-N comparably to CaP-S, while CaP-N exhibited a superior dentinal tubule occlusion than CaP-S, forming mineral plugs and depositing new nanoparticles onto demineralized collagen. This behavior was attributed to its bigger particle size and increased solubility. DMA depth profiling and SEM showed an excellent interaction between the newly formed mineralized structures and the pristine tissue, particularly at the exposed collagen fibrils.
Significance: CaP-N demonstrated very good remineralizing and occlusive activity in vitro, *comparable to CaP-S, thus could be a promising circular economy alternative therapeutic agent for dentistry.*

1. Introduction

Dental caries was defined in 2017 as the most widespread non-communicable disease, affecting billions of people worldwide [1]. When the pH of the oral microenvironment becomes lower than a critical value – ca. 5.5 for dental enamel and 6.2 for dentin – the mineral constituent of the tooth, hydroxyapatite (HA, $Ca_{10}(PO_4)_6(OH)_2$), starts to dissolve [2]. The main factors for this phenomenon are the metabolism of cariogenic bacteria, the consumption of acidic foods, and gastroesophageal reflux disease (GERD) [3]. The consequence of demineralization is the formation of an ionic imbalance on the tooth surface, causing progressive loss of Ca^{2+} and PO_4^{3-} ions and tissue degradation.

Demineralization is a reversible process, and if (i) the pH of the oral microenvironment is higher than the critical values and (ii) free Ca^{2+} and PO_4^{3-} ions are available, the ionic balance is inverted and remineralization of the depleted tissues occurs [4]. In ideal physiological conditions, saliva provides ions and buffering effect, stimulating remineralization. Unfortunately, this activity is insufficient to contrast and restore demineralization generated by cariogenic bacteria [3]; thus,

* Corresponding author.
E-mail address: michele.iafisco@issmc.cnr.it (M. Iafisco).

https://doi.org/10.1016/j.dental.2024.02.019
Received 23 October 2023; Received in revised form 2 February 2024; Accepted 12 February 2024
Available online 16 February 2024

an external supply of calcium and phosphate ions is required to shift the equilibrium toward remineralization [5,6]. Naturally, among most common remineralizing agents are calcium phosphate (CaP) materials [7], which have a chemical composition similar to that of dental hard tissues [8]. Most frequently, CaPs are represented by synthetic HA nanoparticles. Nano-HA has been proven to have excellent action as it releases remineralizing ions and adheres to tooth surface, restoring demineralized lesions [9,10]. In addition, HA nanoparticles can contrast dentin hypersensitivity by occluding exposed dentinal tubules and forming a mineralized barrier [11].

In the last few years, it has been proposed that synthetic CaPs could be complemented or substituted by CaPs from natural sources following a circular economy approach [12,13]. Food industries produce millions of tons of by-products per year, whose disposal is a severe environmental and economic issue [14]. However, these by-products contain valuable compounds, e.g., CaPs of bones from slaughterhouses or fisheries. In this case, the circular economy approach consists in the extraction and valorization of these CaPs, having the benefits of decreasing the amounts of by-products sent to incinerators and landfills and providing an added economic value to otherwise useless materials [13,15].

Several natural sources that could yield CaPs have been investigated [13]. In particular, there is a high interest in CaPs from marine sources, as the fish food industry produces large quantities of by-products – e.g., European fisheries produce about 3.1 million tons of by-products per year – that are rich in CaPs (fish scales and bones) [14,16,17]. Our research group has recently studied the extraction of CaPs from salmon fish bones (hereafter referred to as CaP-N, being derived from a natural source) by thermal treatment as an effective and easily scalable method [18]. Advanced applications of CaP-N include UV-scattering agents, nutrient delivery agents, and dye adsorbent phases for water remediation [18–20]. As a consequence of extraction through thermal treatment, CaP-N consists of a biphasic mixture of β-tricalcium phosphate (β-TCP, β-form of $Ca_3(PO_4)_2$) and HA [18]. This biphasic composition suggests that CaP-N might be an attractive material for dental remineralization and desensitization. β-TCP is more soluble than HA both in neutral and acidic conditions [21]; thus, CaP-N could have substantial ion release for stimulating remineralization while having at the same time the economic and environmental benefits of being from circular economy sources. Synthetic mixtures of HA and β-TCP similar to CaP-N are known as biphasic calcium phosphates (BCP) and were successfully employed in orthopedics as material for bone substitution [22]. However, to the best of our knowledge, no study has investigated the use of BCP on dental hard tissues. Few recent works have used HA from fish by-products for dental applications such as dental resin composite fillers or enamel remineralization [23–25]. However, these works have employed pure HA minerals, not BCPs. All these reasons make CaP-N a potentially attractive but still unexplored alternative to synthetic CaPs for dental application.

The present work tested circular economy CaP-N as occlusive agent of dentinal tubules and enamel remineralization agent. The null hypothesis was the absence of remineralizing action on demineralized enamel and dentine and the absence of occlusive action on dentinal tubules. A synthetic stoichiometric nano-HA (CaP-S) was used as a positive control of remineralization and occlusion, while water was used as a negative control.

2. Materials and methods

2.1. Materials

Calcium hydroxide ($Ca(OH)_2$, 95% pure), lactic acid ($C_3O_4H_6$, 85 wt % in H_2O), Dulbecco's modified phosphate buffered saline (Dulbecco's modified PBS without $CaCl_2$ and $MgCl_2$, composition: KCl 0.2 g/L, KH_2PO_4 0.2 g/L, Na_2HPO_4 1.15 g/L, NaCl 8.0 g/L), orthophosphoric acid (H_3PO_4, 85 wt% in H_2O), and sodium lactate solution ($NaC_3O_4H_5$, 50 wt% in H_2O) were purchased from Sigma Aldrich (St. Luis, MO, USA). All the solutions were prepared with ultrapure water (18.2 MΩ × cm at 25 °C, Arium pro, Sartorius, Göttingen, Germany).

2.2. Preparation and characterization of CaP-N and CaP-S

CaP-N was prepared from salmon fish bones, as reported by Adamiano *et al.* [19]. Briefly, clean and dry salmon fish bones were thermally treated at 800 °C with a heating ramp of 120 °C h^{-1} and 1 h of dwell time, then ground with a jet mill (PilotMill-2, Food and Pharma Systems s.r.l., Como, Italy) and sieved with a 20 μm sieve.

As reported in a previous work, CaP-S was synthesized by wet precipitation to obtain nanosized HA [26], where the nominal molar Ca/P ratio was set to the stoichiometric value of 1.67. Briefly, 30 mL of an aqueous solution of phosphoric acid (H_3PO_4, 8.87 g) was added drop-wise into 100 mL of calcium hydroxide ($Ca(OH)_2$, 10.00 g) water suspension kept under stirring at room temperature and atmospheric conditions. After adding the acid, the suspension was stirred for 3 h and left overnight before recovering the synthesis product by centrifugation. The obtained material was repeatedly washed with ultrapure water and freeze-dried overnight.

For both CaP-N and CaP-S, powder X-ray diffraction (PXRD) patterns were recorded with a D8 Advance Diffractometer (Bruker, Karlsruhe, Germany) equipped with a Lynx-eye position sensitive detector, using the CuKα radiation (λ = 1.54178 Å) generated at 40 kV and 40 mA. PXRD patterns were acquired in the 10 - 60° (2θ) range with a step size of 0.02° and a scanning speed of 0.5 s. Crystal phase quantification was performed through Rietveld refinement with the software TOPAS5 [27] considering a multiphase system and using tabulated atomic coordinates of HA (ASTM Card file No. 00–009-0432) and β-TCP (ASTM Card file No. 00–009-0169). All acquisitions were performed in triplicate.

The chemical composition of the materials was analyzed on three replicates for each sample using an inductively coupled plasma optical emission spectrometer (ICP-OES) (Agilent 5100, Agilent Technologies, Santa Clara, CA, USA). Before analysis, 10 mg of samples were dissolved in 50 mL of 2 wt% HNO_3 solution. The Ca, P, and Mg content of the samples were measured by their atomic emission at the following wavelengths: 422.673 nm for Ca, 213.618 nm for P, and 279.553 nm for Mg.

The materials' morphology and particle dimension were evaluated by field-emission gun scanning electron microscopy (FEG-SEM) (ΣIGMA, ZEISS NTS Gmbh, Oberkochen, Germany). Powders were mounted on aluminum stubs using an adhesive carbon tape and sputter-coated with an 80:20 Pt:Pd alloy in an E5100 Sputter Coater (Polaron Equipment, Watford, Hertfordshire, UK) to improve the electrical conductance. Micrographs were collected at 4 kV acceleration voltage in secondary electron mode at 2500 × - 100,000 × magnifications.

2.3. Ion release from CaP samples and characterization of materials after release

Cumulative ion release tests from the tested CaP materials were performed as reported by Degli Esposti *et al.* [28] with some modifications. In detail, slurries of either CaP-S or CaP-N were made by mixing 2 g of dry powders with 6 mL of ultrapure water (pH 7.0) or 0.1 M lactic acid solution (pH 4.5) in triplicate and incubated at 37 °C under horizontal agitation. After 30 min, 2 h, 6 h, 24 h, 3 d, and 7 d the materials were centrifuged (7000 rpm, 4 °C, 5 min), and 4.8 mL of the supernatant was collected and replaced with an equal volume of fresh solution. The pH of the supernatants was measured, then the supernatants were diluted 1:5 with 2 wt% HNO_3 solution and analyzed by ICP-OES to quantify the content of Ca, P, and Mg.

To assess changes to CaPs during ion release, additional samples prepared in the same conditions were centrifuged after 7 d of incubation, and the pelleted material was freeze-dried. PXRD and FEG-SEM analyses of the dried powders were performed as reported above.

2.4. In vitro evaluation of enamel remineralization and dentinal tubules occlusion

Enamel remineralization and dentinal tubules occlusion in vitro tests were performed as reported by Ionescu *et al.* [5]. In brief, a total of 6 sound (caries-free) erupted human wisdom teeth extracted for clinical reasons were obtained (Oral Surgery Unit, Department of Biomedical, Surgical and Dental Sciences, Milan, Italy) and used for the in vitro experiments. The Ethical Commission of the University of Milan approved the use of the teeth (codename: SALTiBO–2017). All in vitro experiments were performed in accordance with the Declaration of Helsinki, updated by the World Medical Association in 2013. Horizontal sections of the teeth specimens were obtained under constant water cooling using a low-speed saw (Isomet 1000, Buehler, Lake Bluff, IL, USA). First, the crown was sectioned from the root with a cut 2 mm apical to the cementoenamel junction. Then, horizontal cuts of the crown were performed at two depth levels to obtain flat enamel (n = 6) and dentin (n = 6) surfaces from each tooth (Fig. 1A). Then, on both dentin and enamel sections, two parallel 0.5 mm-deep notches were made on the top surface of each specimen to mark three areas using a low-speed diamond disc (Horico, Berlin, Germany) (Fig. 1B). All surfaces were polished using silicon carbide paper (600 and 1200 grit). The surfaces were etched with a 37 wt% H_3PO_4 solution for 30 s, followed by extensive rinsing with filter-sterile tap water to generate a superficial demineralization comparable to a white spot lesion of enamel [29].

Before each treatment, an aliquot of CaP-N or CaP-S dry powder was mixed with ultrapure water to obtain a 25 wt% aqueous slurry. The three regions of each enamel or dentin specimen were soft-brushed for 3 min using disposable microbrushes (Microbrush, Microbrush International, Grafton, WI, USA) with (i) CaP-N slurry, (ii) CaP-S slurry (positive control), and (iii) filter-sterile tap water (negative control); the distribution of groups in the three regions of each specimen was randomized (Fig. 1C). After brushing a single region, the specimen was rinsed with filtered sterile tap water for 1 min to stop exposure to the CaP sample. In total, 6 regions of enamel and 6 regions of dentin were brushed with each sample group.

This treatment was repeated twice daily for one week; the slurries were prepared fresh for each treatment. Specimens were stored at 37 °C in fresh Dulbecco's modified PBS (formulation without calcium and magnesium to avoid precipitation of calcium phosphates unrelated to treatments). After the last treatment, half of the specimens (n = 3 for both enamel and dentin) destined for FEG-SEM analysis were dehydrated by immersion in ethanol solution with progressively higher concentrations (35%, 70%, 80%, 90%, and 100% twice) for 5 min each, then left to dry overnight. The remaining specimens were stored under 100% humidity until instrumented indentation tests (Fig. 1D).

The dried specimens were fixed on aluminum stubs using conductive graphitic glue with the treated surface upward to observe surface morphology. All specimens were sputter-coated as described above and observed with the FEG-SEM instrument equipped with an EDS probe (INCA Energy 300, Oxford Instruments, Abingdon-on-Thames, UK) in secondary electrons mode at an acceleration voltage of 4 kV. For each specimen and treatment, at least four randomly selected fields were acquired at magnifications ranging from 2500 × to 100,000 × .

For dentin samples, the occlusion of dentinal tubule openings was quantified by digital image analysis of FEG-SEM micrographs using the method reported by Ahmed *et al.* and the open image processing package Fiji [30,31]. For each treated sample, at least six 5000 × micrographs were acquired, noise was removed by the despeckling process, and then the black openings were selected by adjusting black/white threshold levels. Afterward, the "analyze particles" Fiji plugin was used to measure the opening area. A total of 300 distinct measurements were performed.

Energy-dispersive spectroscopy (EDS) surface compositional analysis was performed with an acceleration voltage of 15 kV. Immediately before sample analysis, the EDS instrument was calibrated by measuring the spectrum of a NIST standard sample of metallic cobalt as suggested by the instrument manufacturer. Six randomly selected fields were acquired for each specimen/treatment combination at 2500 × magnification in full-frame mode using an acquisition time of 50 s. Each field represented a volume area of 10 × 10 x ≈ 1 μm (thickness) of the specimen surface.

After these observations, specimens were carefully detached from the stubs, and a 0.2 mm-deep vertical notch was made on the surface opposite the treated region. Then, a section running through the

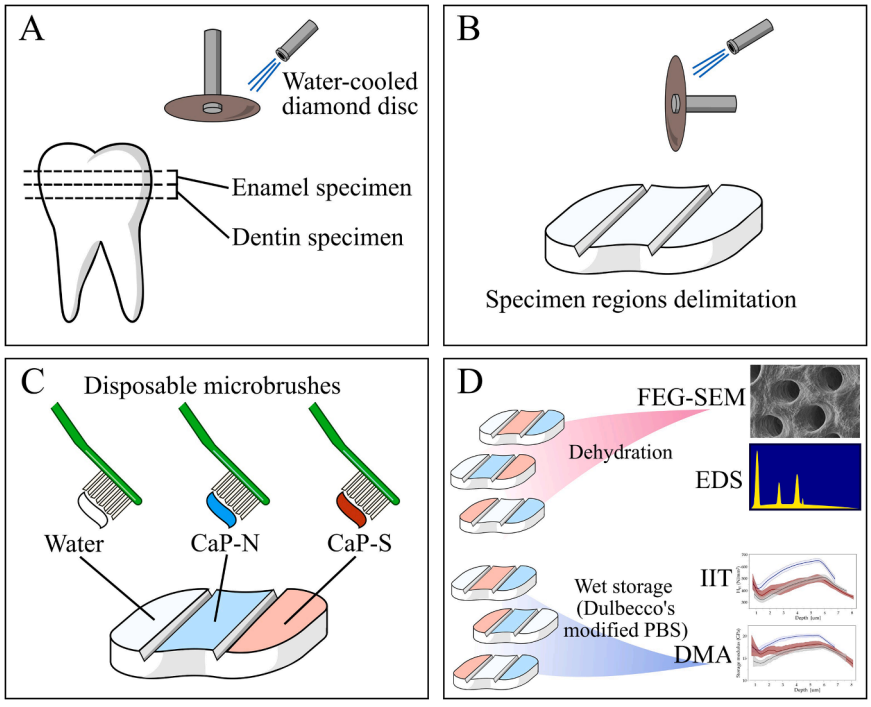

Fig. 1. Schematic representation of specimen preparation and treatment. (A) Horizontal sectioning of the tooth to expose enamel and dentin, (B) delimitation of regions by parallel notches, (C) randomized treatment with negative control and samples, (D) post-treatment specimen preparation for characterizations.

remineralized layer of enamel and dentin specimens was obtained through fracturing by applying pressure on a 0.2 mm steel wedge placed in the notch. Extreme care was taken through these procedures not to touch the fractured surface to avoid the presence of dirt or artifacts. Finally, the fractured sections were mounted again on aluminum stubs with the fractured surface upward, sputtered, and observed again with the FEG-SEM.

2.5. Instrumented indentation test (IIT)

The ratio of the elastic reverse deformation work of indentation (W_{elast}) and the total mechanical work of indentation (W_{total}) was assessed ($W_{elast}/W_{total} = \mu_{IT}$) according to ISO 14577 [32] by using an automated micro-indenter (FISCHERSCOPE® HM2000) equipped with a Vickers diamond tip. This parameter (μ_{IT}) is a prerequisite for the dynamic mechanical analysis (DMA) test. For this purpose, 10 measurements were carried out randomly in the dentin and enamel reference specimens under wet conditions. Inside each notch that was created on the specimens' surfaces, a thin cotton thread was placed and connected on both ends to small containers filled with Dulbecco's modified PBS. Thus, the specimen under test was kept from desiccating due to capillarity through the thread. This method allowed to maintain hydrated the specimens during analysis as the instrument cannot operate on completely submerged specimens. The indentation was force-controlled and at room temperature; the test load increased within 20 s and decreased within 20 s with constant speed in the 0.4 mN to 500 mN range. Load (F) and indentation depth (h) of the indenter were continuously measured during the load-unload-cycle, allowing calculating the elastic and plastic deformation. A part of the mechanical work, Wtotal (= Fdh), during the indentation procedure is consumed as plastic deformation work (W_{plast}), while the rest is set free as work of the reverse elastic deformation ($W_{elastic}$). During indentation, an impression is produced with a projected area of contact of the indenter (A_c) determined from the force/indentation depth curve, taking into account the indenter correction based on the Oliver and Pharr model and described in ISO 14577 [32]. The indenter area function was calibrated on two materials with uniform and well-known properties (sapphire and fused quartz). Corrections obtained from the tip calibration are then used for further computational data evaluation. The indentation hardness ($H_{IT} = F_{max}/A_c$) is calculated from the maximum force and the projected contact area and represents a measure of the resistance to plastic deformation. This value is convertible to HV (Vickers hardness). The indentation modulus (E_{IT}) was then calculated from the slope of the tangent of the indentation depth-curve at maximum force [32].

2.5.1. Dynamic mechanical analysis (DMA)

The DMA analysis involved a quasistatic force applied in 20 steps varying in the load cycle from 10 mN to 500 mN. Upon reaching each step interval, a low magnitude oscillating force (1.0 Hz) was superimposed on the quasistatic force. The oscillation amplitude was set at 5 nm, so the sample deformation was kept within the linear viscoelastic regime. For each tooth substrate and treatment, 20 indentations were performed randomly.

For the used frequency (1.0 Hz), the force oscillation generates oscillations on the displacement signal with a phase angle δ. The sinusoidal response signal was then separated into real and imaginary parts representing the storage (E′) and the loss moduli (E″), respectively. E′ is a measure of the elastic response of material behavior, whereas E″, characterizes the viscous material behavior. The quotient E″/ E′ is defined as the loss factor (tan δ) and is a measure of the material damping behavior.

2.6. Statistical analysis

Structural and compositional analyses of the materials were performed in triplicate and repeated at least three times. Results are reported as the mean of the three experiments ± 1 standard deviations.

EDS data of enamel and dentin surfaces were analyzed to compare the quantity of each element between the CaP-treated regions against negative control. One-way ANOVA and Tukey-Kramer's HSD multiple comparisons post-hoc tests were applied for $p < 0.05$.

Data regarding dentinal tubule opening areas obtained by FEG-SEM image analysis had a non-normal distribution. Therefore, they were analyzed by applying the Mann-Whitney U test comparing the opening area of CaP-treated regions vs. negative control and setting the significance level to $p < 0.05$.

Data were log-transformed for each microhardness parameter of the enamel surfaces, except tan δ, to approximate normal distribution. Data were first analyzed as overall means comparisons for the treatment groups on enamel and dentin using one-way ANOVA and Tukey-Kramer's HSD ($p < 0.05$). After that, curves were plotted considering the variation of each indentation parameter against the indentation depth using the locally estimated scatterplot smoothing (LOESS) method for regression, adjusting for alpha smoothing parameter (range: 0.5 – 0.65) and setting robustness to 1.0 on each parameter to re-weight and de-emphasize the points that are farther from the fitted curve. Confidence intervals of the estimate were also computed.

3. Results

3.1. Characterization of CaP materials

The PXRD patterns of CaP-N and CaP-S are reported in Fig. 2A. Peak indexing shows that CaP-N is a biphasic mixture of 33 wt% HA and 67 wt%, β-TCP, as estimated by Rietveld refinement. For both CaP-N's crystalline phases, the diffraction peaks are narrow and intense, indicating a high level of crystallinity. CaP-S, on the other hand, is made of pure and stoichiometric HA, and its peaks are broad and poorly defined, indicating a low level of crystallinity and the presence of nanocrystals.

These observations were confirmed by FEG-SEM analysis (Fig. 2B,C). Micrographs of CaP-N (Fig. 2B) show that the material is composed of rounded particles ranging from 200 nm to 1 μm. In the case of CaP-S, micrographs (Fig. 2C) illustrate that the material is composed of nanometric elongated particles, < 100 nm long and < 50 nm wide. Both submicrometric CaP-N and nanometric CaP-S particles tend to aggregate into micrometric grains when they are in a dry state.

The chemical composition of the two materials is reported in Table 1. Both CaP-N and CaP-S are almost mainly composed of Ca and P, containing only traces of magnesium (< 1.0 or < 0.2 wt%, respectively).

The evolution over time of CaP-N and CaP-S as a concentrated slurry (25 wt%) in neutral (pH 7.0) or acidic (pH 4.5) aqueous solutions was studied. Both materials increased the environmental pH in the acidic solution despite repeated washouts (Fig. 3A). CaP-N neutralized the acidic solution, while CaP-S leveled at 6.0–6.5. When immersed in the pH 7.0 solution, the two materials showed a different behavior, as CaP-N raised the pH to ≈ 11.0 while CaP-S did not alter the pH significantly (Fig. 3B).

Cumulative ion release curves of the sample slurries in the two solutions expressed as the absolute concentration of ions in the solution and as the weight percentage of ions released are reported in Fig. 4. Unsurprisingly, Ca release (Fig. 4A) was more intense when both CaP materials were in contact with the pH 4.5 solution than under neutral pH conditions. CaP-N at pH 4.5 had a burst calcium release in the first 6 h of incubation and then leveled off after 24 h, while CaP-S release is less intense but steadier so that the release was still present after 7 days. At pH 7.0, the differences between materials were less evident, with a slightly higher Ca release for CaP-S. The P release (Fig. 4B) was also pH-dependent and higher at acidic pH. Both CaP materials showed a relatively intense release of Mg compared to Ca and P, especially under acidic conditions (Fig. 4C).

After 7 days of incubation, PXRD patterns (Fig. 5A) and their Rietveld refinements show that the HA content of CaP-N increased while β-TCP content decreased independently from solution pH (Table 2). In

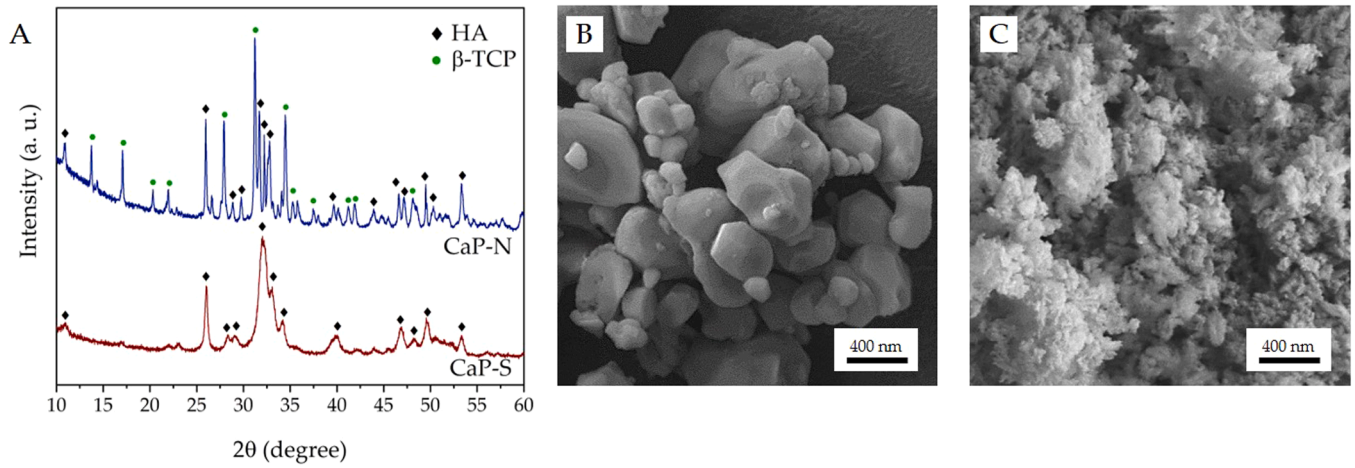

Fig. 2. (A) PXRD patterns of CaP-N and CaP-S; (B-C) FEG-SEM micrographs of (B) CaP-N and (C) CaP-S.

Table 1
Chemical composition of CaP samples.

Material	Ca (wt%)	P (wt%)	Mg (wt%)	Ca/P (mol)	(Ca+Mg)/P (mol)
CaP-N	33.9 ± 0.9	18.0 ± 0.6	0.69 ± 0.02	1.46 ± 0.01	1.50 ± 0.02
CaP-S	34.6 ± 1.0	16.1 ± 0.4	0.14 ± 0.01	1.66 ± 0.01	1.67 ± 0.01

detail, CaP-N was composed by ca. 45 wt% HA in comparison to 33 wt% HA of the pristine material. CaP-S had no changes with incubation. FEG-SEM micrographs of CaP-N after incubation (Fig. 5B,C) showed that new nanometric particles ≈ 100 nm long and 50 nm wide appeared onto CaP-N independently from solution pH. In contrast, no significant morphological changes in CaP-S were observed (Fig. 5D,E).

3.2. Dentin tubules occlusion and enamel remineralization

3.2.1. Dentin tubules occlusion

FEG-SEM showed open and demineralized tubules in the negative control sample (Fig. 6A,D). Single collagen fibrils can be discerned at higher magnification with their characteristic 67 nm-banded structure (Fig. 6G). In contrast, dentin treated with CaP-N (Fig. 6B,E) shows an almost complete occlusion of tubule openings. A similar result was obtained with CaP-S treatment (Fig. 6C,F). The occlusion of dentinal tubule openings (Fig. 6L) as quantified by digital image analysis showed an average tubule opening area of 4 – 8 μm^2 (2 – 3 μm diameter) in the negative control, while for CaP-N, the opening area was reduced to 0.3 – 0.9 μm^2 (0.6 – 1 μm diameter), indicating a statistically significant high occlusion ($p < 0.05$). CaP-S treated region had an opening area of 0.3 – 2.1 μm^2, (0.6 – 1.6 μm diameter), showing a less intense occlusion compared to CaP-N ($p < 0.05$). High magnification micrographs of CaP-N treated samples (Fig. 6H) showed the presence of two types of particles on the dentin surface: (i) rounded particles < 1 μm in size together with (ii) new small and irregular particles < 100 nm in size evenly covering the dentinal surface (marked in Fig. 6E with a green and a light blue arrow, respectively). The high magnification micrographs of dentin after CaP-S treatment (Fig. 6I) show that the dentinal surface is covered by nanoparticles.

FEG-SEM observation of fractured dentin specimens allowed to assess the penetration of CaP materials within the dentinal tubules (Fig. 7). Control specimen tubules were found entirely open, where demineralization involved the first micrometers below the exposed surface (Fig. 7A, D). CaP-N particles were found inside the tubules up to 4 μm depth. In addition, some sparse 1–2 μm thick mineral plugs could be observed obliterating tubule surface opening (Fig. 7E). CaP particles and mineral plugs could also be seen in the dentin specimens treated with CaP-S (Figs. 7C and F, respectively). In this case, the mineral plug was a deposition of CaP-S nanoparticles (marked by green arrows in

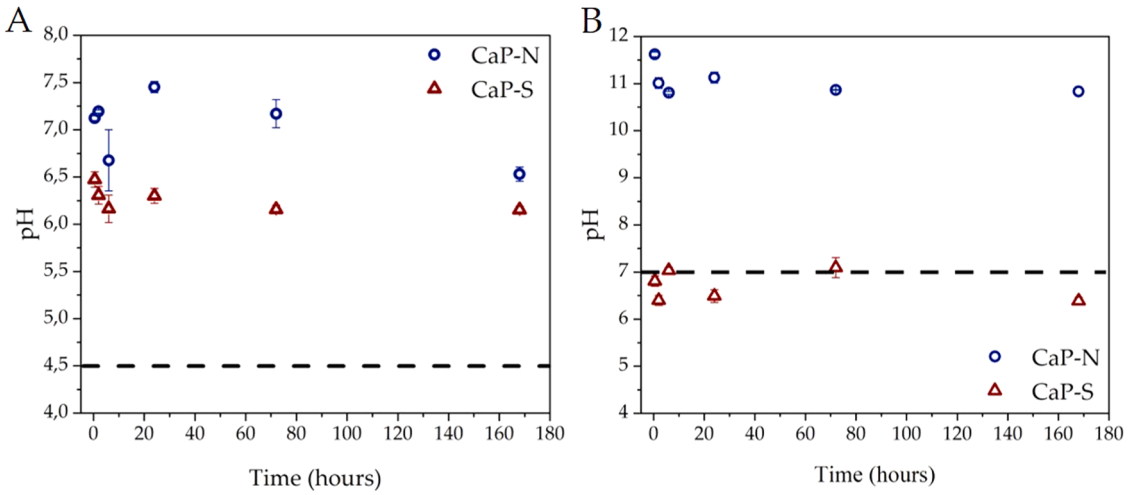

Fig. 3. Evolution over time of pH in (**A**) acidic or (**B**) neutral solutions. The dashed line indicates the pH of the solutions after each refresh.

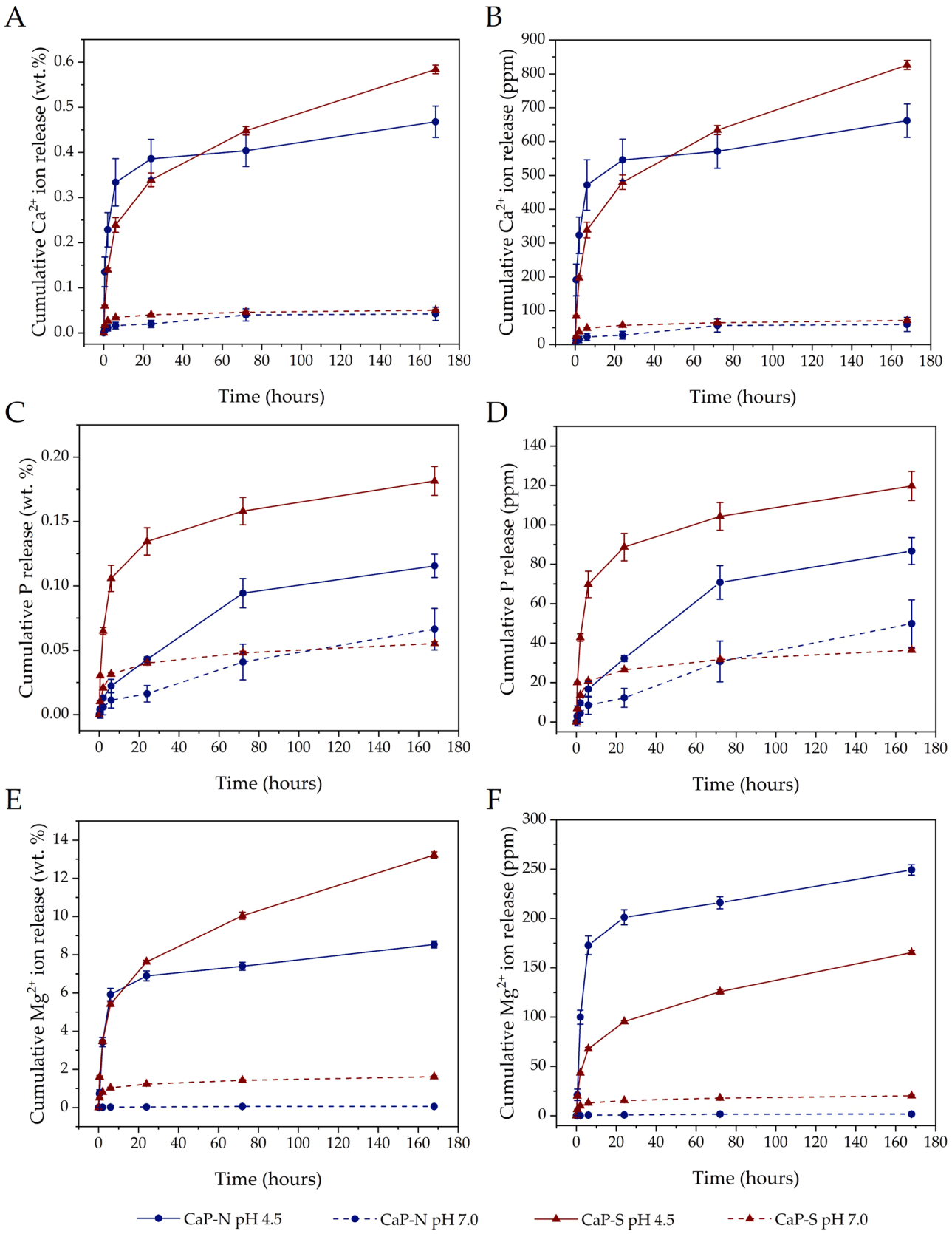

Fig. 4. Cumulative ion release curves for (A,B) Ca, (C,D) P, and (E,F) Mg expressed as (A,C,E) relative weight percentage or as (B,D,F) absolute concentration (ppm).

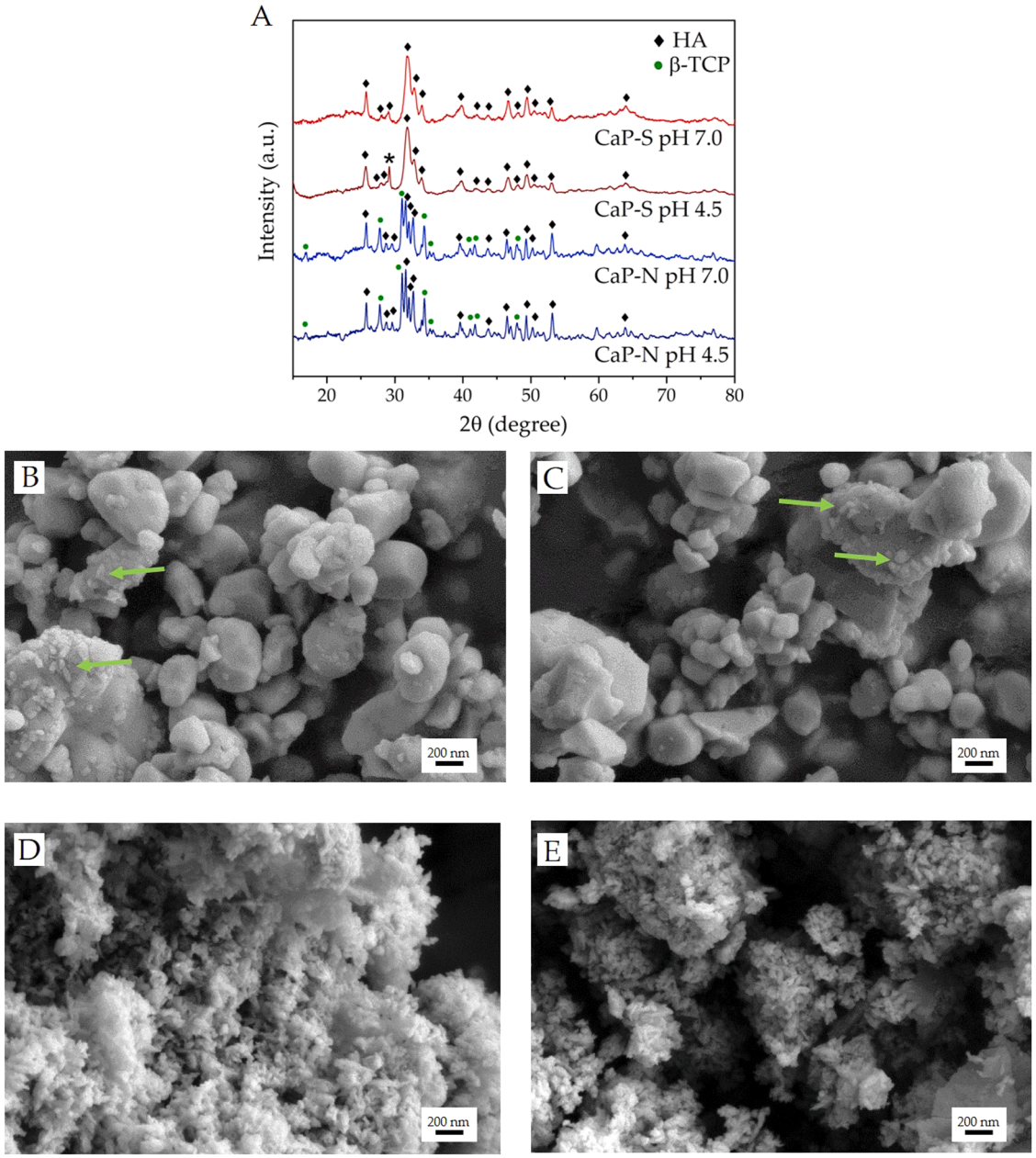

Fig. 5. (A) PXRD patterns of CaP samples after 7 days of incubation in solutions at pH 4.5 or 7.0. The CaP-S samples exposed to the pH 4.5 buffer presented an additional diffraction peak (marked with an asterisk symbol) that might be related to crystalline lactate salts precipitated during incubation. (B-E) FEG-SEM micrographs of CaP-N after 7 days of incubation in (B) acidic or (C) neutral buffer in comparison to CaP-S after 7 days of incubation in (D) acidic or (E) neutral buffer. Green arrows in panels (B, C) highlight the newly formed nanoparticles.

Table 2
Crystal phase composition of CaP samples before and after incubation for 7 days in acidic or neutral solutions.

Material	pH	HA (wt%)	β-TCP (wt%)
CaP-N	As prepared	33.1 ± 0.4	66.9 ± 0.4
	4.5	43.2 ± 0.3	56.8 ± 0.3
	7.0	47.7 ± 0.3	52.3 ± 0.3
CaP-S	As prepared	100	-
	4.5	100	-
	7.0	100	-

Fig. 7C,F).

The chemical composition of dentin surfaces was assessed through elemental quantification by SEM-EDS calibrated with a metallic Co NIST standard (Fig. 8). This approach, previously used for chemical composition analysis of enamel surfaces treated with remineralizing toothpastes, provides a reliable elemental composition of the first micrometers of surface [5]. All specimens contained Ca, O, P, and C; in some cases, traces of Mg were also detected. Ca and P contents were shallow in the negative control, while a significantly higher amount was present in the regions treated with CaP-N ($p < 0.05$). The treatment with CaP-S induced a significant increase of Ca and P compared to the control, albeit to a lower extent than CaP-N ($p < 0.05$). The Ca/P ratio of the negative control dentin surface (Fig. 8D) was 1.16, while CaP-treated samples had a ratio of 1.45 for CaP-N and 1.68 for CaP-S.

Regarding the mechanical behavior, the quasistatic indentation test determined the indentation hardness and indentation modulus (referred to as H_{IT} and E_{IT}, respectively). Both tested CaPs improved dentin's resistance to plastic deformation (Fig. 9A-D). The improvement was

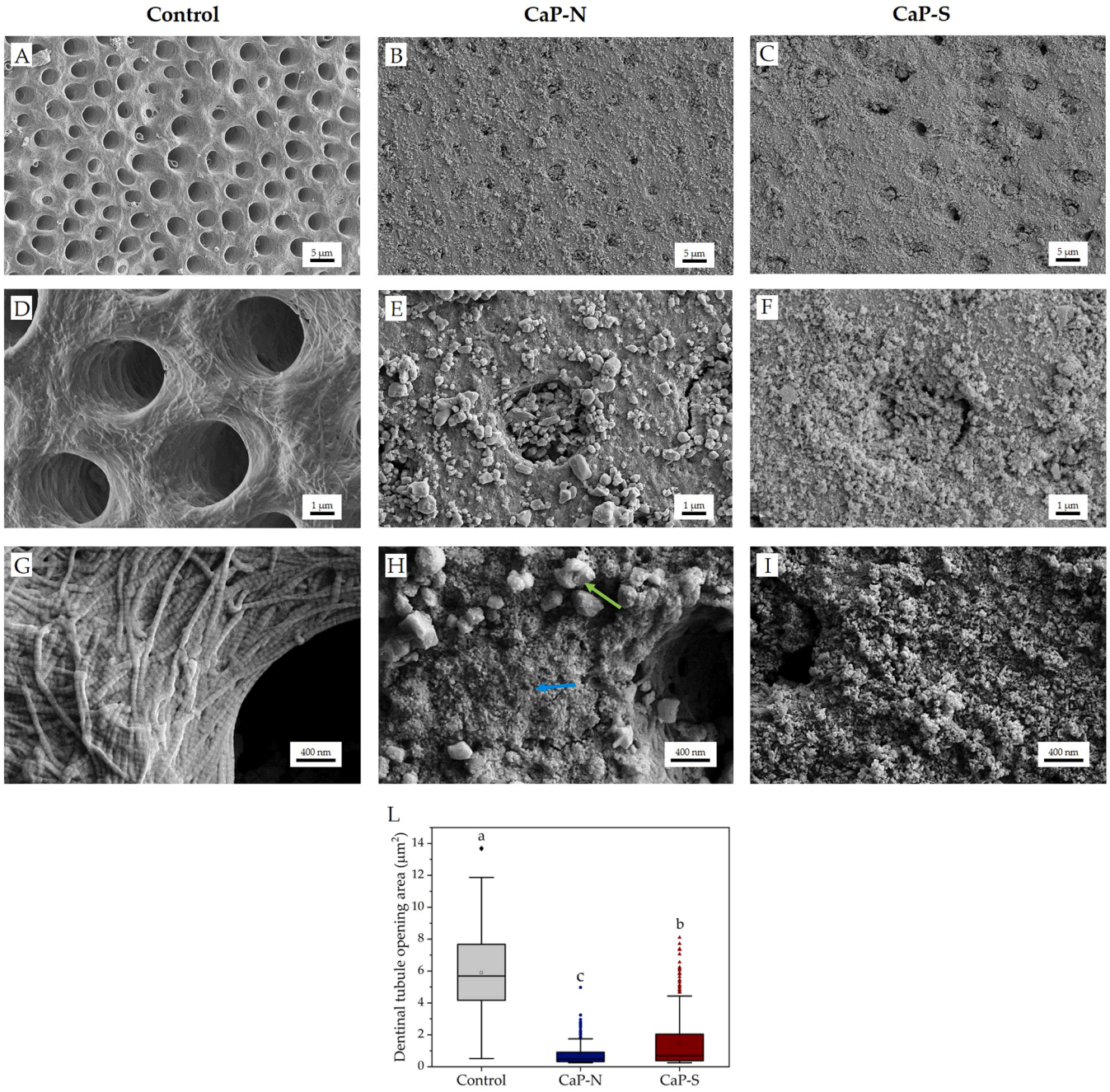

Fig. 6. FEG-SEM micrographs of demineralized dentin surfaces after treatment with (A,D,G) water, (B,E,H) CaP-N and (C,F,I) CaP-S. (L) Tubule occlusion quantification by digital image analysis. The green arrow in panel (H) highlights CaP-N particles, while the light blue arrow highlights the newly formed mineral phase deposited onto the dentin surface. Different superscript letters in panel (L) represent statistically different groups ($p < 0.05$).

depth-dependent, and the materials showed different behaviors. CaP-N increased H_{IT} by about 50% compared to the negative control up to a depth of 6 µm (Fig. 9A) and increased E_{IT} by about 25% up to the same depth (Fig. 9C). CaP-S showed the highest E_{IT} value in the first 0.5 µm of depth, and for the following 2.5 µm of depth, a H_{IT} and E_{IT} higher than the negative control but lower than CaP-N (Fig. 9A, C). At depths > 2.5 µm, there was no difference between CaP-S and control.

DMA was used to study the viscoelastic behavior of CaP-treated dentin compared to the negative control (Fig. 9E-L). The storage modulus of dentin treated with the tested CaP materials in function of depth was similar to the indentation hardness curve (Fig. 9E,F). Both treatments increased the storage modulus, with CaP-S showing a significant increase up to 2.5 µm depth, while CaP-N reached 6.5 µm. Both CaP treatments also significantly increased loss modulus up to 7 µm depth, and no significant difference between the behavior of the treatments was highlighted (Fig. 9G,H). Regarding tan δ, CaP-N slightly decreased this parameter, while CaP-S slightly increased it compared to the negative control; this effect was not depth-dependent (Fig. 9I,L).

3.2.2. *Enamel remineralization*

FEG-SEM micrographs of the negative control show initial demineralization of the enamel surface (Fig. 10A, D). At higher magnification, voids are formed between the prisms due to the dissolution of the interprismatic mineral phase, which is usually more prone to demineralization being less crystalline. After treatment with CaP-N (Fig. 10B), the enamel surface displayed a continuous aspect without interprismatic

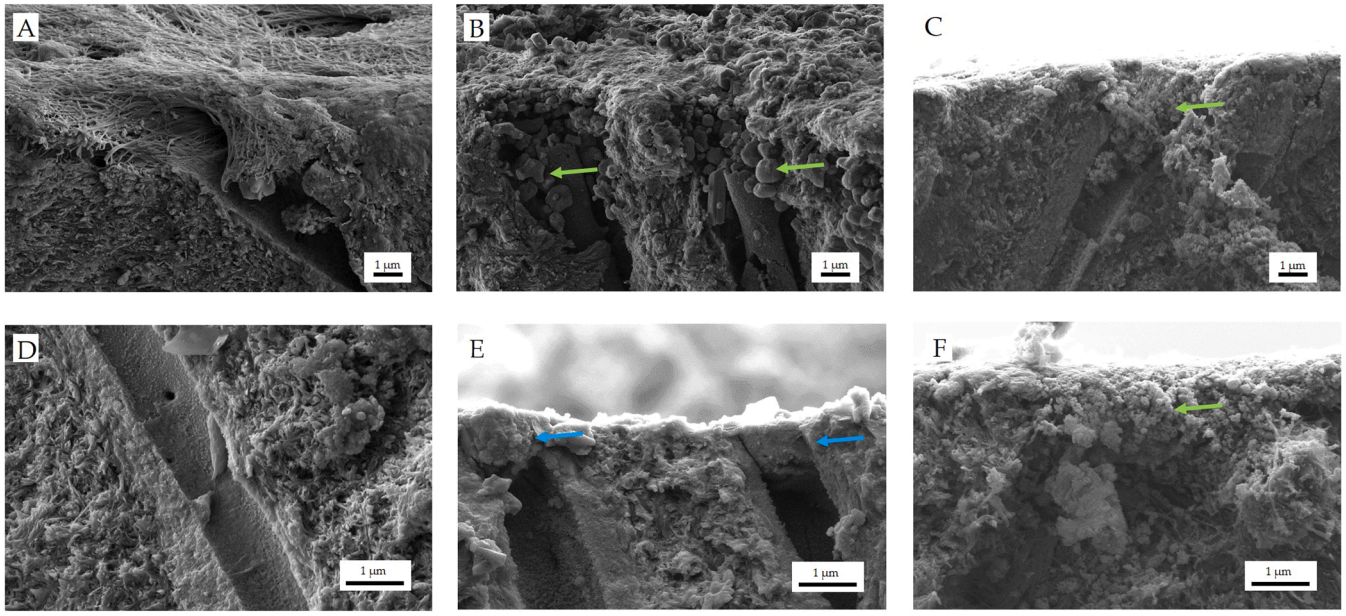

Fig. 7. FEG-SEM micrographs of demineralized dentin sections after treatment with (A,D) water, (B,E) CaP-N and (C,F) CaP-S. Green arrows in panels (B, C, F) highlight the CaP particles deposited within dentinal tubules, while the light blue arrows in panel (E) highlight the newly-formed mineral plugs. In panel (**B**), the cylindrical residues of Tomes fibers present in dentin at the moment of treatment can be observed.

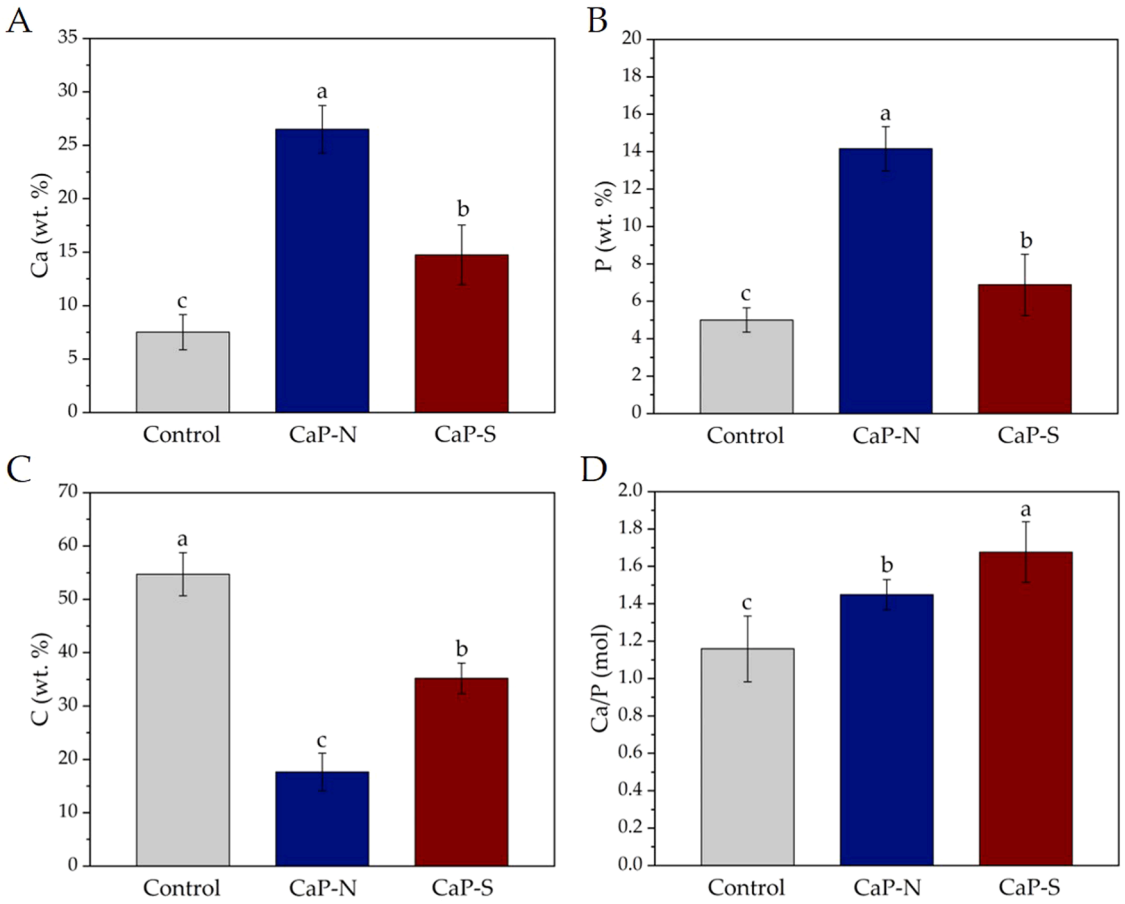

Fig. 8. SEM-EDS measurement of (A) Ca and (B) P, and (C) C content and (D) Ca/P molar ratio of dentin surfaces after treatment. Different superscript letters in each panel represent statistically different groups ($p < 0.05$).

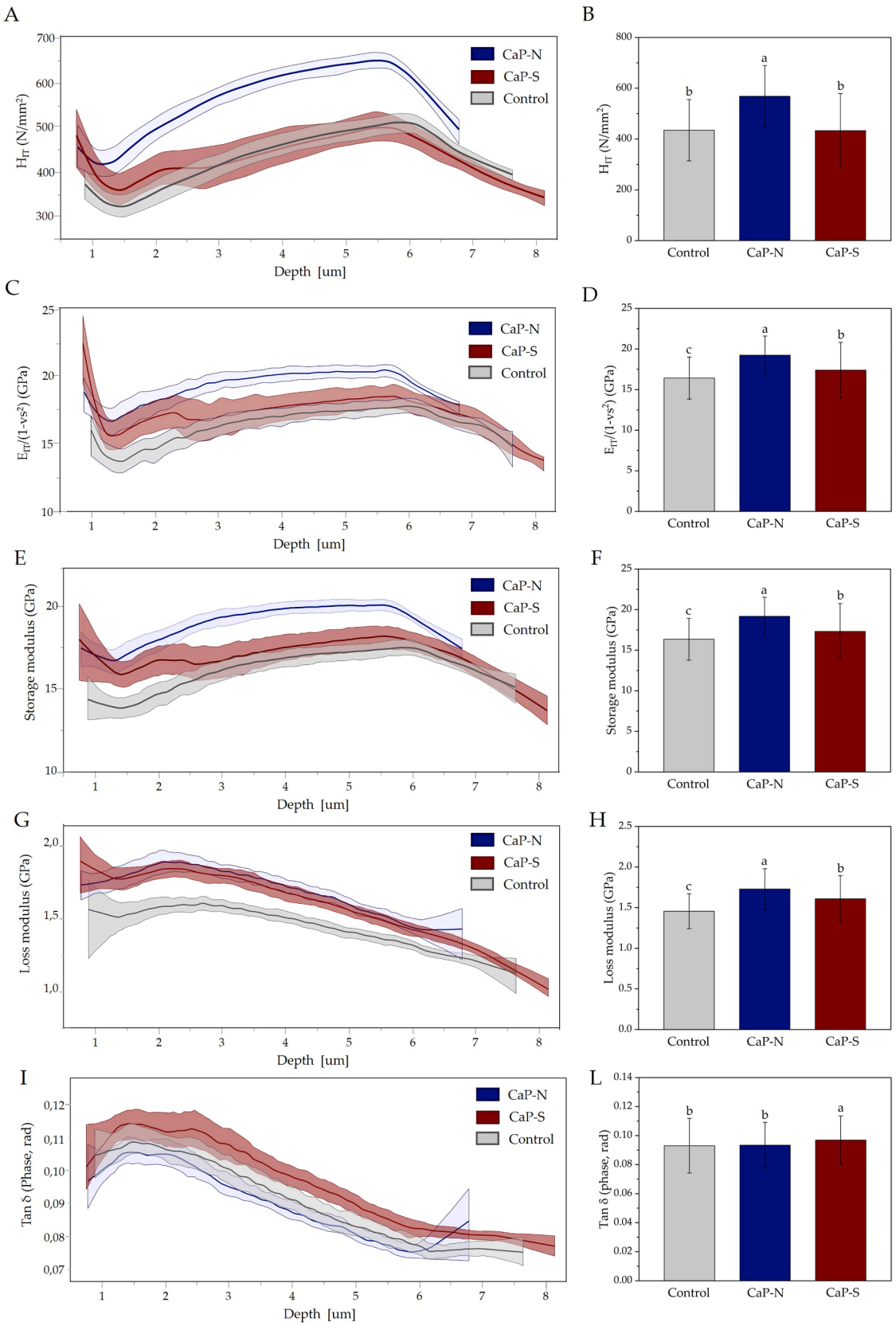

Fig. 9. (A-D) Quasistatic indentation parameters of dentin surfaces after treatment. (A) Indentation hardness as a function of indentation depth and (B) average indentation hardness. (C) Indentation modulus as a function of indentation depth and (D) average indentation modulus. (E-L) Viscoelasticity parameters of enamel surfaces after treatment. (E) Storage modulus as a function of indentation depth and (F) average storage modulus. (G) Loss modulus as a function of indentation depth and (H) average loss modulus. (I) Tan δ as a function of indentation depth and (L) average tan δ. Different superscript letters in panels (B,D,F,G,L) represent statistically different groups. Note that panels show reverse-transformed data while statistics were performed on log-transformed data.

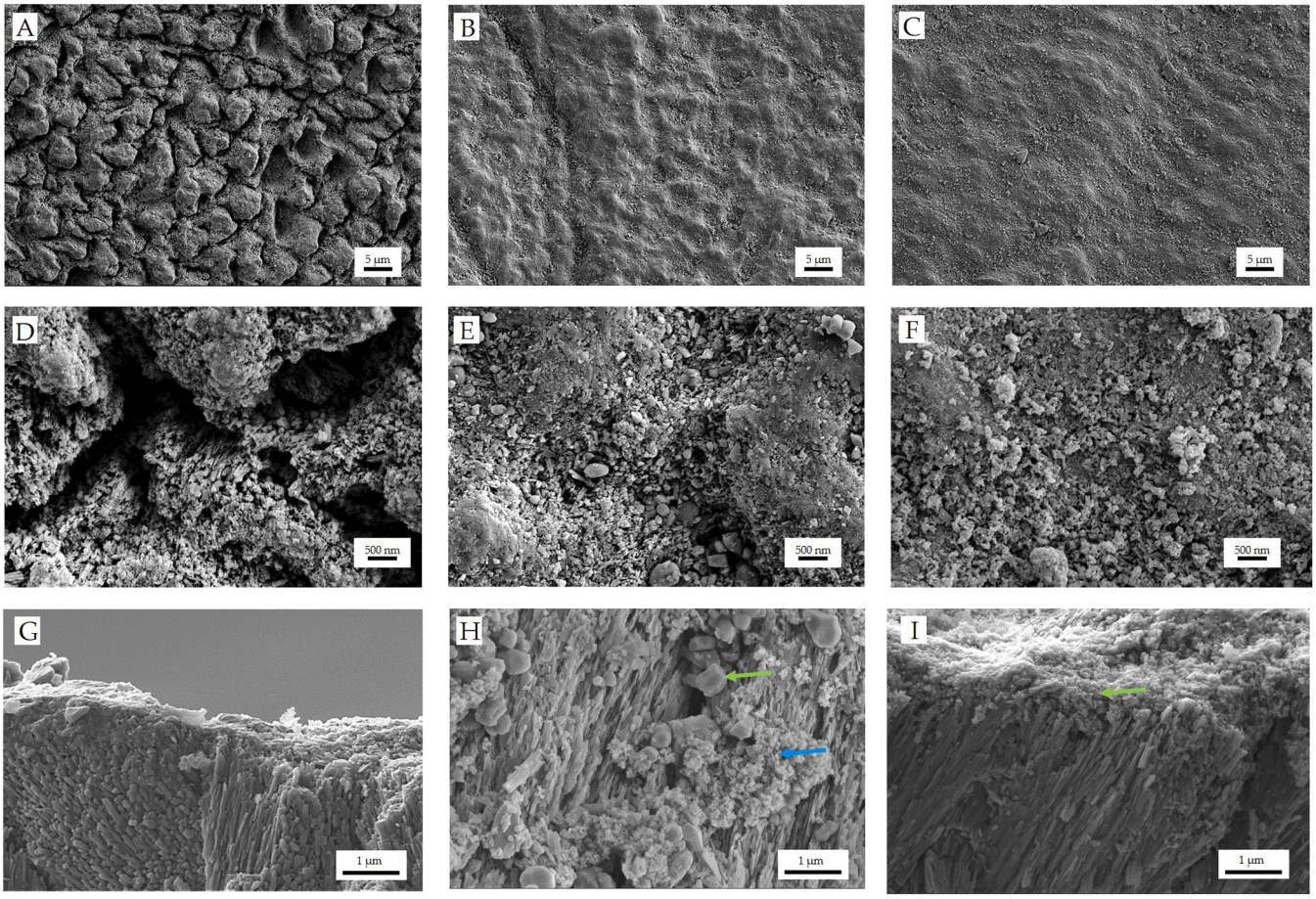

Fig. 10. (A-F) FEG-SEM micrographs of the demineralized enamel surfaces after treatment with (A,D) water, (B,E) CaP-N, or (C,F) CaP-S. (G-I) Micrographs of demineralized enamel prism sections after treatment with (G) water, (H) CaP-,N, or (I) CaP-S. Green arrows in panels (H, I) highlight the CaP particles deposited within enamel prisms, while the light blue arrows in panel (H) highlight the newly-formed nanoparticles.

voids. High-magnification micrographs (Fig. 10E) reveal the deposit of CaP-N particles and newly formed nanoparticles in the interprismatic region. A similar effect was observed after treatment with CaP-S (Fig. 10C); in this case, the stoichiometric HA nanoparticles filled interprismatic voids and deposited onto the enamel surface (Fig. 10F).

FEG-SEM micrographs of the sectioned enamel specimens are displayed in Fig. 10G-I. The negative control showed the typical structure of enamel tissue (Fig. 10G), including HA prisms arranged into staggered rows showing interlocking and offsetting of prism heads. CaP-N treated samples (Fig. 10H) showed CaP-N particles deposited between prisms together with newly formed nanoparticles. The micrographs of CaP-S treated regions (Fig. 10I) showed a similar outcome, with the deposition of nanoparticles mainly in the interprismatic space.

SEM-EDS (Fig. 11) of the negative control mainly showed Ca, O, and P signals with traces of Mg. There was no statistically significant difference in Ca or P content between the control and treated surfaces ($p > 0.05$). Also, Ca/P molar ratios were not statistically different ($p > 0.05$).

Hardness parameters of the quasistatic indentation test showed that both tested CaPs improved enamel's resistance to plastic deformation (Fig. 12A-D), yet CaP-N had a distinctly higher effect than CaP-S up to 2.5 µm depth. The negative control showed an initial high hardness

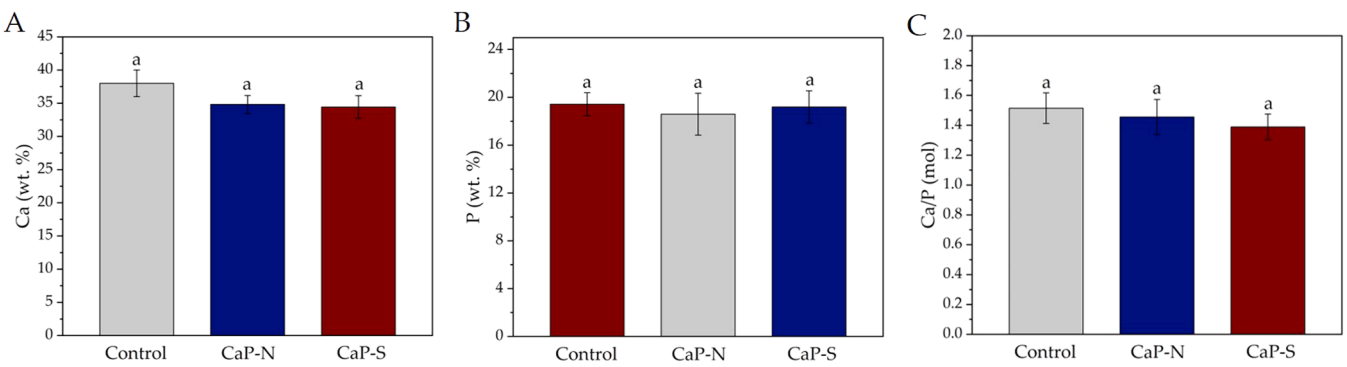

Fig. 11. SEM-EDS measurement of (A) Ca and (B) P, and (C) Ca/P molar ratio of enamel surfaces after treatment. Different superscript letters in each panel represent statistically different groups ($p < 0.05$).

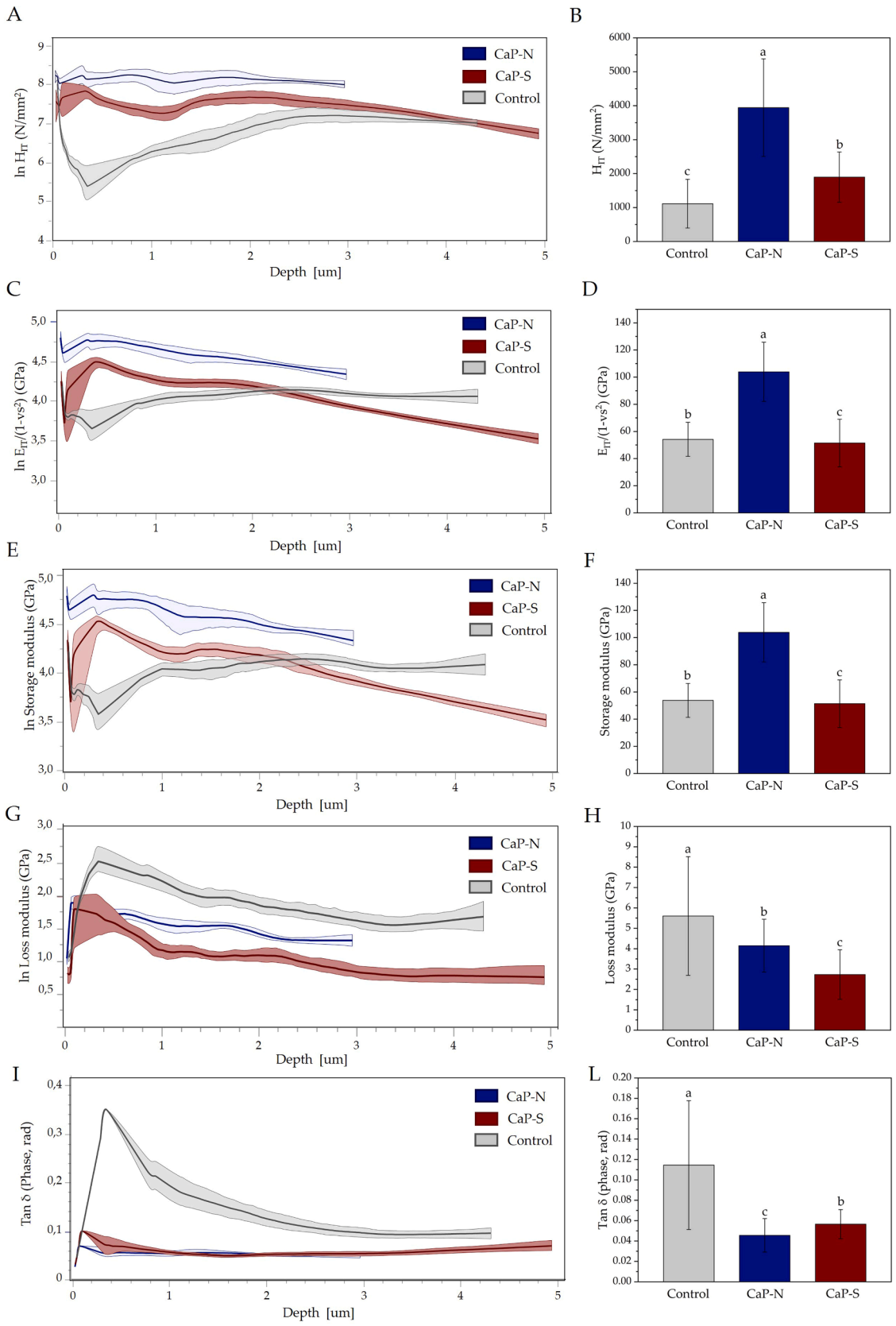

Fig. 12. (A-D) Quasistatic indentation parameters of enamel surfaces after treatment. (A) Indentation hardness as a function of indentation depth and (B) average indentation hardness. (C) Indentation modulus as a function of indentation depth and (D) average indentation modulus. (E-L) Viscoelasticity parameters of enamel surfaces after treatment. (E) Storage modulus as a function of indentation depth and (F) average storage modulus. (G) Loss modulus as a function of indentation depth and (H) average loss modulus. (I) Tan δ as a function of indentation depth and (L) average Tan δ. Different superscript letters in panels (B,D,F,G,L) represent statistically different groups. Note that panels show reverse-transformed data while statistics were performed on log-transformed data.

value at the enamel surface level (< 0.1 μm) and then swiftly decreased in the first 0.5 μm to be slowly restored, reaching 3.0 μm depth. Similarly to H_{IT} and E_{IT}, both tested CaPs increased enamel storage modulus (Fig. 12E,F). Both CaP treatments decreased the loss modulus compared to the negative control, with CaP-S producing a higher effect than CaP-N (Fig. 12G,H). The consequence was that both CaPs sharply decreased the tan δ value compared to the control, flattening the tan δ curve concerning the probing depth (Fig. 12I,L).

4. Discussion

The present work aimed to test a CaP material derived from fish industry circular economy to be used as dentine tubules occlusion and enamel remineralization agent. The characterization of CaP-N showed that it occurs as a biphasic mixture of HA and β-TCP, confirming previous findings [18]. The presence of β-TCP is due to the calcination of fish bones' calcium-deficient biogenic HA (i.e., with a Ca/P molar ratio < 1.67), as at temperatures above 700 °C Ca-deficient HA partially recrystallizes into the β-TCP phase, as widely reported in the literature [33]. Thermal treatment leads to the formation of a highly crystalline material characterized by a round particle morphology due to partial grain growth and sintering during the heating and to β-TCP recrystallization, in agreement with previous reports on the thermal treatment of fish bones [34]. In contrast, CaP-S is poorly crystalline and characterized by a nano-morphology that imparts a high specific surface area, typical of HA synthesized by wet precipitation in the selected conditions [35]. The Ca and P content and their molar ratio for CaP-N are in good agreement with the values reported for other thermally-treated fish bones [36,37]. At the same time, Mg is more abundant in CaP-N than CaP-S as HA from marine biogenic sources is often cation-substituted [33]. Overall, material characterization revealed that CaP-N differed from stoichiometric nano-HA (CaP-S) in terms of particle size, morphology, crystallinity, and phase composition, suggesting that very different behavior may arise when these two materials are supplied to dental hard tissues.

CaP-N behavior in an acidic aqueous solution showed that it could efficiently buffer the acidic environment as effectively as CaP-S, stabilizing the pH at neutral values. It is well reported in literature that CaP materials dissolve at low pH, releasing PO_4^{3-} ions, which in turn form a phosphate buffer at pH ca. 6–7 [38]. This pH-dependent solubility is proved by the experiments of ions release. Over time, the ions release in the acidic solution tends to level off due to the increase of pH, which in turn decreases dissolution. Differently, in a neutral aqueous solution, CaP-S does not affect pH, while CaP-N increases it significantly. This behavior may be attributed to the presence of traces of calcium oxide (CaO) on CaP-N particles' surface in amounts that cannot be detected by PXRD (< 0.5 wt%). CaO formation is a by-product of thermal treatment of non-stoichiometric carbonate-doped apatites due to carbonate decomposition, and this occurrence has been previously reported for calcined pig bones [39,40]. In water, CaO hydrates to calcium hydroxide, which is a base. Hence, in water the increase of pH was likely due to the presence of CaO traces in the concentrated CaP-N suspension (25 wt %). Nevertheless, an alkaline environment is not detrimental to dental tissues, as a comparable pH is generated by mineral trioxide aggregate (MTA), which is commonly used in endodontic treatment as a root repair material and does not cause harmful effects [41]. Moreover, due to CaO presence, CaP-N neutralizes the acidic solution to pH 7.0–7.5 while CaP-S buffers the pH at a lower value of 6.0–6.5.

The faster calcium release of CaP-N compared to CaP-S may be related to the presence of β-TCP phase, which is more soluble than HA and thus could release a significant amount of Ca^{2+} ions [22]. Because of β-TCP solubility, CaP-N quickly shifts solution pH to higher values than CaP-S. Regarding the relatively high Mg release of both CaP materials, we hypothesize that their Mg-rich regions dissolved preferentially, as Mg^{2+} distorts HA crystal lattice, decreasing crystallinity and thus resistance to acidic dissolution. It is of particular interest that CaP-N, after 7 days of incubation, had a lower β-TCP content and formed new nanoparticles independently from the solution pH. This data confirms a preferential dissolution of the more soluble β-TCP phase, in agreement with the literature [21], that induced the precipitation of new CaP minerals. In contrast, CaP-S did not show any significant change with incubation.

Based on these preliminary data, we decided to test the behavior of CaP-N in terms of dentinal tubule occlusion and enamel remineralization using protocols and experimental conditions that simulated the clinical use as closely as possible. To compensate for the intrinsic variability of enamel and dentine surfaces and avoid using a high number of replicates, the three experimental groups (treatment with water/CaP-N/CaP-S) have been applied randomly on separate regions of the same tooth slice. CaP-N treatment led to an excellent occlusion of tubule openings and the formation of mineral plugs at the sub-surface level. This result indicates that the sub-micrometric granules of CaP-N (200 nm – 1 μm) are small enough to penetrate and occlude dentinal tubules, which usually range from 1 to 3 μm in size for tooth sections taken close to dentin-enamel junction [42]. In addition, the observation highlighted the presence of deposited CaP-N particles (rounded particles < 1 μm in size) together with a newly deposited nano-structured mineral phase. These small nanoparticles were not present in pristine CaP-N powder (Fig. 2B) or in dentin (Fig. 6A, D, G) but were very similar to the ones that formed when CaP-N was incubated in an aqueous slurry (Fig. 5B, C). Therefore, it is likely that they have formed in situ. An interpretation is that during treatment, CaP-N particles adhered to the partially demineralized dentin, releasing Ca^{2+} and PO_4^{3-} ions over time, and then such ions interacted with the exposed collagen, inducing a new mineral phase deposition. This finding suggests that treatment with CaP-N can stimulate dentin remineralization. SEM-EDS data confirm the collagen-based dentin remineralization, as the negative control has a low Ca and P content and a high C content, mainly due to the exposed collagen. At the same time, these values are inverted after treatment with CaP-N. In addition, the fact that the Ca/P ratio of the dentin specimens treated with either CaP-N or CaP-S matches their respective Ca/P ratios confirms that the mineral observed in the outer dentin layer is primarily due to deposited CaP materials.

In the case of CaP-S, FEG-SEM, and SEM-EDS, data show that a carpet of nanoparticles evenly covers the dentinal surface. However, it is impossible to determine whether this mineral layer is due to the direct deposition of CaP-S nanoparticles or a new mineral phase induced by CaP-S. CaP-S treatment achieved a penetration depth comparable to CaP-N within dentin tubules and could induce the formation of mineral plugs, although with a slightly lower efficiency. These findings suggest that CaP-N and CaP-S might have different mechanisms of action when applied to dentin. In the case of CaP-N, its bigger particles can easily obstruct the tubule and get stuck in the first two microns of the tubule depth, as the tubule diameter corresponds to the size of about 2–4 particles. Then, the release of ions stimulated the remineralization of the demineralized dentin tissue, inducing the formation of thick plugs. For CaP-S particles, their nanometric size may lead to a diffusion deep inside the tubule, which in turn achieves an overall lower tubule occlusion. However, if enough particles are repeatedly administered, they can effectively obstruct the opening and form a mineral plug over time.

All dentinal hypersensitivity treatments aim to close the exposed dentinal tubules quickly and permanently. However, if the intertubular dentinal collagen is not simultaneously remineralized, the exposed dentin may become a region of reduced hardness prone to mechanical failure [43]. For this reason, it is of paramount importance to look at the mechanical behavior of the dentin exposed to the remineralizing treatment to better understand the efficacy of such procedures. The micro-indentation data suggest that CaP-N and CaP-S could both improve dentin's mechanical characteristics. In particular, CaP-N provided a homogeneous increase of the tissue hardness as a function of dentin depth. In contrast, CaP-S provided a very high hardness increase at the dentin surface and within the first two micrometers of depth. Variations

in the mechanical properties within the dentin, such as the ones found in the CaP-S treated samples, mean an increased risk of cracking and breakdown of the substrate when an external force is applied, as low modulus regions (below 2.5 μm) lead to energy concentration in high elastic modulus regions (above 2.5 μm) [44]. From this point of view, treatment with CaP-N might be considered a better choice over CaP-S since the latter may concentrate the stress at the very surface where the remineralizing layer is formed, posing a higher risk for fracture at the interface of the newly formed layer.

We used DMA to study the viscoelastic behavior of CaP-treated dentin, as it is a complex composite biomaterial exhibiting both viscous and elastic components when it undergoes deformation. The viscoelasticity of the bulk dentin matrix represents the interaction between the collagen fibrils, collagen crosslinking and density, associated proteoglycans, and the mineral phase [45,46]. The first parameter is the storage modulus, representing the material's ability to store energy elastically. Both CaP materials increased dentin's storage modulus, with CaP-N positively affecting deeper regions than CaP-S. This stiffening effect could result from the remineralizing activity by the tested treatments, leading to the precipitation of minerals inside the tissue, thus indicating that CaP-N also induced remineralization in deep dentin. On the other hand, the loss modulus represents the material's ability to dissipate stress (viscous behavior). The increase of loss modulus and, thus, the capability to dissipate mechanical energy by both CaP treatments could be due to a large interface area between the collagen fibrils and the newly formed mineral particles of the remineralized structures [47]. Finally, tan δ represents the ratio of the viscous to elastic response of the material, providing information on the overall damping ability or the capacity to absorb shock. The decrease of tan δ values induced by CaP-N treatment in comparison to negative control and the opposite increase by CaP-S can be attributed to particle size. Indeed, the damping behavior is related to the internal friction generated by grain or interphase relaxation, which in CaP-S offers a larger stress dissipation area due to the much smaller particle size than CaP-N. It has been reported that the dissolution of CaP compounds supplied to dentin creates an ions-rich environment that induces dentin remineralization, which is reflected in a decrease of tan δ and increased storage and loss modules in the material [48]. Therefore, a possible interpretation of the DMA data is that both tested CaPs induced nucleation and growth of nanocrystals into dentin, remineralizing it, and the treatment induced an excellent connection between the newly formed mineralized structures and the pristine tissue, in particular with the exposed collagen fibrils.

Altogether, our data demonstrates that CaP-N is a very promising material for dentin remineralization and occlusion of dentinal tubules, improving the mechanical characteristics of the tissue. CaP-N treatment on dentin can be considered at least as effective as stoichiometric HA nanoparticles, which is an excellent material for this application. Future works will assess the effect of prolonged CaP-N treatments, evaluating the formation of the mineral plugs and their resistance to repeated acidic lesions caused by physiological and pathological pH changes in the oral microenvironment. Moreover, the hydraulic conductance of dentine after long-term treatment with CaP-N should also be assessed to further corroborate the tubules occlusion efficacy.

We also evaluated the efficacy of CaP-N as a material for enamel remineralization. FEG-SEM observation indicated that the treatment, similarly to CaP-S, induced enamel remineralization by deposition into interprismatic defects and stimulated the formation of a new crystalline phase in direct contact with the pristine one.

Quasistatic indentation and DMA tests of the negative control showed that the maximal decrease in hardness and storage modulus was localized in a sub-surface zone within the first micrometer of depth. This observation matches clinical data on initial enamel demineralization lesions (white spots), where a demineralized sub-surface region can be observed underneath an otherwise intact superficial enamel layer. Both CaP materials and mainly CaP-N improved hardness parameters and storage modulus, showing that they could remineralize subsurface enamel layers. In addition, CaP treatments sharply decreased the enamel's tan δ values. Healthy, highly mineralized enamel has a tan $\delta < 0.1$; higher values indicate an excessive viscous behavior caused by demineralized tissue. Therefore, our viscoelastic measurements indicate that both treatments could restore the subsurface enamel lesions by creating a structure that tightly connects with the pristine one, effectively remineralizing the tissue and restoring its mechanical characteristics. The generated enamel lesions had a shallow depth (≤ 3.0 μm) due to the demineralization protocol applied; thus, the lesion depth was shallower than dentin, possibly impacting the evaluation of the activity of the tested CaP materials. In future works, different demineralization protocols (e.g., 48 h at pH 3.5–4.0 [49]) will be applied to test the efficacy of CaP materials on simulated early caries under conditions more closely resembling clinical ones.

In the present study, the experiments were designed to avoid specimen dehydration and consequent artifacts and misinterpretations when performing the microindentation measurements. Also, the choice of the storage medium (Dulbecco's modified PBS) was made to replicate conditions occurring in the external environment. Dulbecco's modified PBS more closely simulates such an environment compared to a simulated body fluid that is commonly used to test biomaterials' behavior when placed inside the human body. For the same reason, specimens were observed without the use of any chemical fixation or collagen degradation inhibition, that would have affected the micromechanical parameters of the tested specimens. In the latter case, the instrumentation would have measured the effect of the fixative on the substrate rather than the effect of the tested treatments. It is clear from the results of the present study that mechanical characteristics differed between tested treatments in a depth-dependent manner. If surface degradation occurred, some difference would have been expected and noticeable in the depth profile as occurring on the outermost layers mainly.

5. Conclusions

Both CaP treatments possessed an excellent remineralizing behavior for initial enamel lesions and dentinal tubules occlusion, and CaP-N has efficacy at least comparable to CaP-S. In addition, CaP-N, due to its different mode of action, could have an edge over CaP-S on dentin desensitization. These findings may suggest using different CaP-based remineralizing agents with tailored remineralization kinetics and mechanisms depending on the specific tissue requirements (i.e., dentine vs. enamel). The findings also show that biphasic calcium phosphate from fish bones, apart from being a more sustainable alternative material, could be a promising circular economy therapeutic agent for dental hard tissues due to its remineralizing and occlusive activity, which will be investigated more in future studies.

Funding

The authors acknowledge the National Research Council (CNR) for providing financial support to this work (Progetti di Ricerca @CNR – avviso 2020 – SEARCULAR).

CRediT authorship contribution statement

Conceptualization, M.I.; methodology, A.C.I.; formal analysis, L.D.E.; investigation, L.D.E., S.G., N.I.; resources, A.C.I.; writing—original draft preparation, L.D.E.; writing—review and editing, L.D.E., A.C.I., S.G., N. I., A.A., E.B., M.I.; visualization, L.D.E.; supervision, M.I. All authors have read and agreed to the published version of the manuscript.

Declaration of Competing Interest

There are no conflicts to declare.

Acknowledgments

All authors gave their final approval and agreed to be accountable for all aspects of the work. They declare no potential economic association and conflicts of interest with respect to the authorship and publication of this paper. We thank Dr. Clara Piccirillo of the Institute of Nanotechnology of Italian National Research Council for performing PXRD patterns of CaP samples after incubation in buffer.

Institutional review board statement

The use of the teeth for the study was conducted in accordance with the Declaration of Helsinki, updated by the World Medical Association in 2013 and approved by the Ethical Commission of the University of Milan (ethical vote number SALTiBO–2017, date of approval, July 11, 2017).

References

[1] James SL, Abate D, Abate KH, Abay SM, Abbafati C, Abbasi N, et al. Global, regional, and national incidence, prevalence, and years lived with disability for 354 diseases and injuries for 195 countries and territories, 1990–2017: a systematic analysis for the Global Burden of Disease Study 2017. Lancet 2018;392:1789–858.
[2] Neel EAA, Aljabo A, Strange A, Ibrahim S, Coathup M, Young AM, et al. Demineralization–remineralization dynamics in teeth and bone. Int J Nanomed 2016;11:4743–63.
[3] Fejerskov O., Nyvad B., Kidd E. Dental caries: the disease and its clinical management: John Wiley & Sons; 2015.
[4] García-Godoy F, Hicks MJ. Maintaining the integrity of the enamel surface: the role of dental biofilm, saliva and preventive agents in enamel demineralization and remineralization. J Am Dent Assoc 2008;139:25S–34S.
[5] Ionescu AC, Degli Esposti L, Iafisco M, Brambilla E. Dental tissue remineralization by bioactive calcium phosphate nanoparticles formulations. Sci Rep 2022;12(1):16.
[6] Cochrane NJ, Cai F, Huq NL, Burrow MF, Reynolds EC. New approaches to enhanced remineralization of tooth enamel. J Dent Res 2010;89:1187–97.
[7] Sauro S, Spagnuolo G, Del Giudice C, Neto DMA, Fechine PB, Chen X, et al. Chemical, structural and cytotoxicity characterisation of experimental fluoride-doped calcium phosphates as promising remineralising materials for dental applications. Dent Mater 2023;39:391–401.
[8] Carella F, Degli Esposti L, Adamiano A, Iafisco M. The use of calcium phosphates in cosmetics, state of the art and future perspectives. Materials 2021;14:6398.
[9] Enax J, Epple M. Synthetic hydroxyapatite as a biomimetic oral care agent. Oral Health Prev Dent 2018;16:7–19.
[10] Melo MAS, Guedes SFF, Xu HHK, Rodrigues LKA. Nanotechnology-based restorative materials for dental caries management. Trends Biotechnol 2013;31:459–67.
[11] Steinert S, Zwanzig K, Doenges H, Kuchenbecker J, Meyer F, Enax J. Daily application of a toothpaste with biomimetic hydroxyapatite and its subjective impact on dentin hypersensitivity, tooth smoothness, tooth whitening, gum bleeding, and feeling of freshness. Biomimetics 2020;5:17.
[12] Russ W, Meyer-Pittroff R. Utilizing waste products from the food production and processing industries. Crit Rev Food Sci Nutr 2004;44:57–62.
[13] Terzioğlu P, Öğüt H, Kalemtaş A. Natural calcium phosphates from fish bones and their potential biomedical applications. Mater Sci Eng: C 2018;91:899–911.
[14] Caldeira C, De Laurentiis V, Corrado S, van Holsteijn F, Sala S. Quantification of food waste per product group along the food supply chain in the European Union: a mass flow analysis. Resour Conserv Recycl 2019;149:479–88.
[15] Ohtake H, Tsuneda S. Phosphorus recovery and recycling. Springer,; 2019.
[16] Ferraro V, Carvalho AP, Piccirillo C, Santos MM, Castro PM, Pintado ME. Extraction of high added value biological compounds from sardine, sardine-type fish and mackerel canning residues—A review. Mater Sci Eng: C 2013;33:3111–20.
[17] Rustad T. Utilisation of marine by-products. Electron J Environ Agric Food Chem 2003;2:458–63.
[18] Adamiano A, Fellet G, Vuerich M, Scarpin D, Carella F, Piccirillo C, et al. Calcium phosphate particles coated with humic substances: a potential plant biostimulant from circular economy. Molecules 2021;26:2810.
[19] Adamiano A, Carella F, Degli Esposti L, Piccirillo C, Iafisco M. Calcium phosphates from fishery byproducts as a booster of the sun protection factor in sunscreens. ACS Biomater Sci Eng 2022.
[20] Falini G, Basile ML, Gandolfi S, Carella F, Guarini G, Degli Esposti L, et al. Natural calcium phosphates from circular economy as adsorbent phases for the remediation of textile industry waste-waters. Ceram Int 2022.
[21] Ebrahimi M, Botelho MG, Dorozhkin SV. Biphasic calcium phosphates bioceramics (HA/TCP): concept, physicochemical properties and the impact of standardization of study protocols in biomaterials research. Mater Sci Eng: C 2017;71:1293–312.
[22] LeGeros R, Lin S, Rohanizadeh R, Mijares D, LeGeros J. Biphasic calcium phosphate bioceramics: preparation, properties and applications. J Mater Sci: Mater Med 2003;14:201–9.
[23] Mathirat A, Dalavi PA, Prabhu A, GV YD, Anil S, Senthilkumar K, et al. Remineralizing potential of natural nano-hydroxyapatite obtained from epinephelus chlorostigma in artificially induced early enamel lesion: an in vitro study. Nanomaterials 2022;12:3993.
[24] Devitasari SP, Hudiyati M, Anastasia D. Effect of hydroxyapatite from waste of tilapia bone (Oreochromis niloticus) on the surface hardness of enamel. J Phys: Conf Ser: IOP Publ 2019:012009.
[25] Razali R, Rahim N, Zainol I, Sharif A. Preparation of dental composite using hydroxyapatite from natural sources and silica. J Phys: Conf Ser: IOP Publ 2018:012050.
[26] Adamiano A, Sangiorgi N, Sprio S, Ruffini A, Sandri M, Sanson A, et al. Biomineralization of a titanium-modified hydroxyapatite semiconductor on conductive wool fibers. J Mater Chem B 2017;5:7608–21.
[27] Coelho A. Topas Academic V5. Coelho Softw 2012.
[28] Degli Esposti L, Ionescu AC, Carella F, Adamiano A, Brambilla E, Iafisco M. Antimicrobial activity of remineralizing ion-doped amorphous calcium phosphates for preventive dentistry. Front Mater 2022;9:846130.
[29] Degli Esposti L, Ionescu AC, Brambilla E, Tampieri A, Iafisco M. Characterization of a toothpaste containing bioactive hydroxyapatites and in vitro evaluation of its efficacy to remineralize enamel and to occlude dentinal tubules. Materials 2020;13(13).
[30] Ahmed T, Mordan N, Gilthorpe M, Gillam D. In vitro quantification of changes in human dentine tubule parameters using SEM and digital analysis. J Oral Rehabil 2005;32:589–97.
[31] Schindelin J, Arganda-Carreras I, Frise E, Kaynig V, Longair M, Pietzsch T, et al. Fiji: an open-source platform for biological-image analysis. Nat Methods 2012;9:676–82.
[32] Standardization IOf. Metallic materials: instrumented indentation test for hardness and materials parameters. Test Method: ISO 2015.
[33] Boutinguiza M, Pou J, Comesaña R, Lusquiños F, De Carlos A, León B. Biological hydroxyapatite obtained from fish bones. Mater Sci Eng: C 2012;32:478–86.
[34] Piccirillo C, Adamiano A, Tobaldi DM, Montalti M, Manzi J, Castro PML, et al. Luminescent calcium phosphate bioceramics doped with europium derived from fish industry byproducts. J Am Ceram Soc 2017;100:3402–14.
[35] Dorozhkin SV. Nanosized and nanocrystalline calcium orthophosphates. Acta Biomater 2010;6:715–34.
[36] Ideia P, Degli Esposti L, Miguel CC, Adamiano A, Iafisco M, Castilho PC. Extraction and characterization of hydroxyapatite-based materials from grey triggerfish skin and black scabbardfish bones. Int J Appl Ceram Technol 2021;18:235–43.
[37] Carella F, Seck M, Degli Esposti L, Diadiou H, Maienza A, Baronti S, et al. Thermal conversion of fish bones into fertilizers and biostimulants for plant growth–A low tech valorization process for the development of circular economy in least developed countries. J Environ Chem Eng 2021;9:104815.
[38] Meyer F, Enax J, Epple M, Amaechi BT, Simader B. Cariogenic biofilms: development, properties, and biomimetic preventive agents. Dent J 2021;9:88.
[39] Merry J, Gibson I, Best S, Bonfield W. Synthesis and characterization of carbonate hydroxyapatite. J Mater Sci: Mater Med 1998;9:779–83.
[40] Sobczak-Kupiec A, Wzorek Z. The influence of calcination parameters on free calcium oxide content in natural hydroxyapatite. Ceram Int 2012;38:641–7.
[41] Torabinejad M, Parirokh M. Mineral trioxide aggregate: a comprehensive literature review—part II: leakage and biocompatibility investigations. J Endod 2010;36:190–202.
[42] Mjör I, Nordahl I. The density and branching of dentinal tubules in human teeth. Arch Oral Biol 1996;41:401–12.
[43] Marshall G, Habelitz S, Gallagher R, Balooch M, Balooch G, Marshall S. Nanomechanical properties of hydrated carious human dentin. J Dent Res 2001;80:1768–71.
[44] Misra A, Spencer P, Marangos O, Wang Y, Katz JL. Micromechanical analysis of dentin/adhesive interface by the finite element method. J Biomed Mater Res Part B: Appl Biomater: J Soc Biomater Jpn Soc Biomater Aust Soc Biomater Korean Soc Biomater 2004;70:56–65.
[45] Farina AP, Vidal CM, Cecchin D, Aguiar TR, Bedran-Russo AK. Structural and biomechanical changes to dentin extracellular matrix following chemical removal of proteoglycans. Odontology 2019;107:316–23.
[46] Matos AB, Reis M, Alania Y, Wu CD, Li W, Bedran-Russo AK. Comparison of collagen features of distinct types of caries-affected dentin. J Dent 2022;127:104310.
[47] Caridade SG, Merino EG, Alves NM, de Zea Bermudez V, Boccaccini AR, Mano JF. Chitosan membranes containing micro or nano-size bioactive glass particles: evolution of biomineralization followed by in situ dynamic mechanical analysis. J Mech Behav Biomed Mater 2013;20:173–83.
[48] Toledano M, Osorio E, Aguilera FS, Osorio MT, Toledano R, López-López MT, et al. Dexamethasone and zinc loaded polymeric nanoparticles reinforce and remineralize coronal dentin. A morpho-histological and dynamic-biomechanical study. Dent Mater 2023;39:41–56.
[49] Sfalcin RA, da Silva JVP, Pessoa VO, Santos J, Olivan SRG, Fernandes KPS, et al. Remineralization of early enamel caries lesions induced by bioactive particles: an in vitro speckle analysis. Photo Photodyn Ther 2019;28:201–9.